Experimental analysis of channel coherence time and fading behavior in the LEO-ground link

Florian Moll (*Author*)
Institute of Communications and Navigation
German Aerospace Center (DLR)
82234 Wessling, Germany
florian.moll@dlr.de

***Abstract*—Characterization and modeling of the optical communication channel in the LEO-ground scenario are a matter of ongoing research. Especially, knowledge about the temporal behavior of the channel is of big importance because it allows development and optimization of channel codes and interleavers to overcome the problem of power fluctuations and thus, signal loss. In this paper, the channel coherence time and fading statistics seen by a 40 cm aperture on ground are experimentally investigated and a modeling approach is given and discussed.**

Keywords—LEO downlink; channel charaterization; channel modelling; atmospheric turbulence; temporal statistics; OICETS

I. INTRODUCTION

Free-space optical communication can satisfy future bandwidth needs for direct downlinks from LEO satellites to ground. However, quality of the optical signal may be degraded heavily due to corruption of spatial coherence while propagating through the turbulent atmosphere. Modeling of this degradation with respect to accuracy and operability (with trade-off between both) is of big importance for the design of a communication system. General theory and models to estimate the effect of turbulence on the laser beam can be found in literature [1][2]. The turbulence effects specifically relevant in the LEO-ground scenario were also investigated [3]. A theoretical and numerical study of the temporal behavior of the turbulence effects in this scenario is given in [4]. However, simplicity of use and description of parameter variability is not always given and more practical, yet physically compliant, models that can also cover parameter variations (as experienced in real measurements) may be helpful. The focus of the actual paper is an analysis of the temporal behavior of signal fluctuations based on recorded measurements during the KIODO (KIrari Optical Downlink to Oberpfaffenhofen) campaigns with the DLR Optical Ground Station Oberpfaffenhofen (OGS-OP) near Munich, Germany and description of a modeling approach using the measurements. The campaigns took place in 2006 and 2009 and are described and – to some extent – analyzed in [5][6][7][8]. LEO-downlink measurements and analysis were also undertaken by NICT, JPL, ESA, and Aerospace Corporation in Tokyo (Japan), Wrightwood (California, USA) and Izania (Tenerife, Spain) [9][10][11]. Measured temporal power spectra of signal fluctuations are given in [11][12]. In the actual paper, measurement results from the KIODO campaigns are given and, with focus on temporal behavior, i.e. channel correlation time and fading statistics, extending the preliminary results presented in an earlier paper [7]. The measurements describe the turbulence behavior for the location of the OGS-OP. However, the results can be translated to a more general formulation applying common theory.

The structure of the paper is as follows: introduction is in chapter 1. Chapter 2 briefly outlines the necessary theory and related equations. The measurement setup is described in chapter 3. The actual results of the measurement campaigns are listed in chapter 4 A (analysis of single satellite pass), chapter 4 B (display of measurement results over link elevation angle) and chapter 4 C (display of measurement results over instantaneous link slew rate). A modeling approach that makes use of the recorded measurements is presented and discussed in chapter 5 and conclusion are drawn in chapter 6.

II. APPLIED THEORY

Intensity fluctuations due to atmospheric turbulence may follow different statistics like log-normal and gamma-gamma distributions [2][13]. Following the experience of [13], it is assumed that in the case of the KIODO measurements with the 40 cm aperture, the received power fluctuations follow a log-normal distribution. Hence, the formulation of fade statistics for log-normal distributed intensity fluctuations, widely applied for weak fluctuation scenarios, can be used as given in [2] and applied for the description of power scintillation. The advantage towards the gamma-gamma model is that for description of the probability density function (PDF), only knowledge of the power scintillation index σ_P^2 [-] is needed as input and not a parameter set for small and large scale fluctuations. The expected number of fades per unit time $\langle n(P_T)\rangle$ [s^{-1}] can thus be written as [2]

$$\left\langle n(P_T)\right\rangle = \nu_0 \exp\left[-\frac{((1/2)\sigma_P^2 - 0.23F_T)^2}{2\sigma_P^2}\right]. \qquad [1]$$

υ_0 [Hz] is the quasi-frequency of the fading process for weak fluctuation conditions [14]. It can be considered as the mean frequency of fades and surges when the signal level and fade threshold have the same value [2] and is given by

$$\nu_0 = \frac{1}{2\pi}\sqrt{-\frac{B_P''(\tau=0)}{B_P(\tau=0)}} = \frac{1}{2\pi}\left(\frac{\int_0^\infty \omega^2 S_P(\omega)d\omega}{\int_0^\infty S_P(\omega)d\omega}\right)^{1/2}. \qquad [2]$$

$B_P(0)$ [P^2] and $B_P''(0)$ [P^2/s^{-2}] are the covariance function of the received power over time and its time derivative evaluated at $\tau = 0$. This is in turn related to the power spectral density of the process $S_P(\omega)$ [P^2/Hz]. With $S_P(\omega)$ being in the integral of the denominator and nominator, the total energy has no influence on the quasi-frequency but the shape of the spectrum. Thus, $\langle n(P_T)\rangle$ is a function of power scintillation index, describing the strength of the scintillation, and the quasi-frequency, describing the fluctuation velocity of the scintillation. The fading threshold F_T [dB] in equation [1] is defined by

$$F_T = 10\log\left(\frac{\langle P_{Rx}\rangle}{P_T}\right), \qquad [3]$$

where $\langle P_{Rx}\rangle$ [W] is the expectation value of received power and P_T [W] the defined fading threshold. The probability of fade (or fractional fade time) $\Pr(P<=P_T)$ is given by [2]

$$\Pr(P \le P_T) = \frac{1}{2}\left\{1+\mathrm{erf}\left[-\frac{(1/2)\sigma_P^2 - 0.23F_T}{\sqrt{2}\sigma_P}\right]\right\}. \qquad [4]$$

$\Pr(P<=P_T)$ shows no time dependency and can therefore be determined just by knowledge of the power scintillation index. With the probability of fades and the expected number of fades, the mean fade length $\langle t(P_T)\rangle$ is calculated [2]:

$$\langle t(P_T)\rangle = \frac{\Pr(P \le P_T)}{\langle n(P_T)\rangle}. \qquad [5]$$

Therefore, determination of the mean fade length needs the power scintillation index and the quasi-frequency.

III. Description of the Measurement System

During the two campaigns, several measurement devices were operated in parallel. The ones of interest here are the applied power meter setups. In 2006, a laboratory PIN sensor was used for power recordings. In 2009, a PIN receiver front-end (RFE) was used. The transmission (measurement) wavelength of the OICETS satellite was 847 nm. An overview of the analyzed measurements is given in TABLE I. All seven measurements were performed in summer during the night between 2 am and 5 am local time.

TABLE I. List of analyzed measurements. The designation contains the year of measurement and sequential numbering of the two campaigns (e.g. KT06-02 corresponds to Kiodo 2006 trial #02). The time corresponds to 1° elevation angle.

Date	*Time [UTC]*	*Exp. designation*
9th June 2006	00:00:24	KT06-02
14th June 2006	01:02:51	KT06-03
15th June 2006	23:52:10	KT06-04
1st July 2009	01:28:12	KT09-03
19th August 2009	02:20:34	KT09-05
21st August 2009	01:02:50	KT09-06
28th August 2009	02:04:38	KT09-08

The most important specifications of the applied measurement setup are given in TABLE II. The recordings were done with 10 kHz and 20 kHz sampling rate, high enough to adequately sample the highest spectral components of power fluctuations. The Cassegrain telescope with 40 cm primary mirror was both time the same. The field of views of the power meters, 0.9 and 0.7 µrad, were much larger than the OGS mount tracking errors of ~50µrad. Therefore, OGS tracking is considered to have no influence on the measurement results.

TABLE II. Most important specifications of the measurement setups in the campaigns 2006 and 2009.

Year	*2006*	*2009*
Meas. wavelength	847 nm	847 nm
Aperture diam.	40 cm	40 cm
Sampling rate	10 kHz	20 kHz
Sensor type	Thorlabs PDA55 Si PIN	RFE Si PIN
Sensor size	3.6x3.6 mm	1.0 mm (diam.)
Field of view	0.9 mrad	0.7 mrad

Tracking errors of the satellite laser terminal LUCE (Laser Utilizing Communications Equipment) are around 2 µrad [10]. With a transmit beam FWHM divergence of 5.5 µrad, also negligible measurement errors are expected. Since the mean captured power changes with elevation angle, together with the fluctuations, the applied power meter must bear a large dynamic range. To increase the dynamic, a variable optical attenuator (automatized neutral density filter wheel), was applied in 2009, enabling the measurements to span a larger range of elevation angles. Signals were recorded by use of a National Instruments DAQ card with 16bit channels. The principle of the measurement setup is illustrated in Fig. 1.

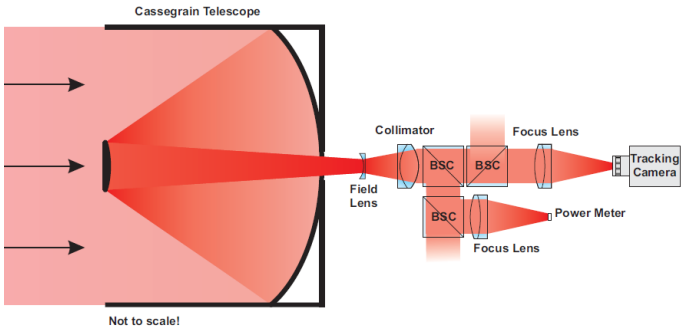

Fig. 1. Principle of optical setup of power measurements. Aside the tracking camera and the power meter, other measurement devices were installed which are indicated with open beam paths.

The light is received with the Cassegrain telescope which forms, together with two lenses (field lens and collimator lens), a beam compressor of factor 1/40. A system of beam splitter cubes (BSC) distributes the power to several beam paths, two out of it being the tracking camera and the power meter (as illustrated in Fig. 1). The preprocessing of the raw data is as follows: noise reduction is performed applying a 2 kHz low-pass filter. Fluctuations beyond are found to be negligible. The systematic offset is removed and cases of low signal to noise ratio and saturation are excluded. Finally, the power records are inspected manually and intervals with preposterous data are detected and also excluded. A sliding window with 1 s length is used for calculation of the specific values. This length is considered to come up with a data base large enough to let the statistics converge but short enough to avoid unwanted averaging. All given statistics in chapter IV are to some part directly derived from the preprocessed power measurement vector and to some part calculated from measurement results. For some parameters both ways are possible and plausibility checks were performed, however, are no matter of discussion here.

IV. MEASUREMENT RESULTS

A. Analysis of a single satellite pass

In this chapter, power fluctuation behavior and fading statistics during a satellite pass are exemplary shown for KT06-04 (15th June 2006, 23:52:10 UTC, 01:52:10 local time). All metrics are displayed over link elevation angle (from 8° to 26°) for uniform comparison. The runs over slew rate will be given in a later chapter to better indicate dependency on satellite motion. The preprocessed power vector is plot in Fig. 2. Arbitrary units are used here because the power meter was not calibrated for absolute measurements. The mean received power increases with elevation (purple line) from (8° to 24°. Around the increasing mean, the power fluctuations can be seen with the black dots. Beyond 24°, the power drops down, probably due to occurrence of a thin cloud in the link of sight. The gaps in the recording are caused by deterministic tracking outages during the satellite overflight.

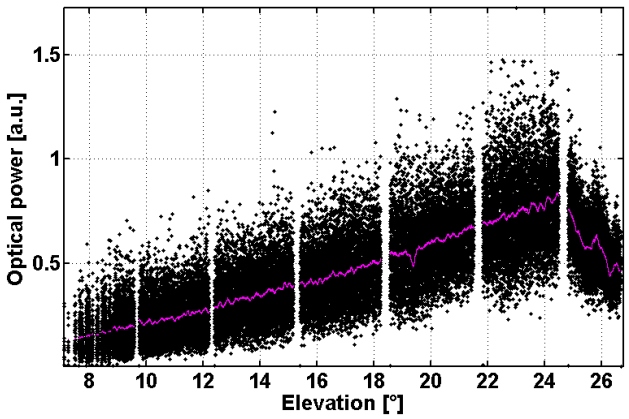

Fig. 2. Received power over elevation at KT06-04 in arbitrary units. The black values are the power samples recorded at 10 kHz. The magenta line is the 1 s sliding window mean [7].

The dependency of fluctuation on link elevation, i.e. length of propagation path through the atmosphere, becomes clearer in Fig. 3. The power is normalized to unity mean revealing the higher fluctuations at low elevation and lower fluctuations at high elevation. A dynamic range of around 15 dB at 8° elevation decreases to a range of 4 dB at 26°. The occurrence of clouds in the link path as seen in Fig. 2 obviously has no influence on the scintillation here. The red dashed line indicates a defined fading threshold of -3 dB.

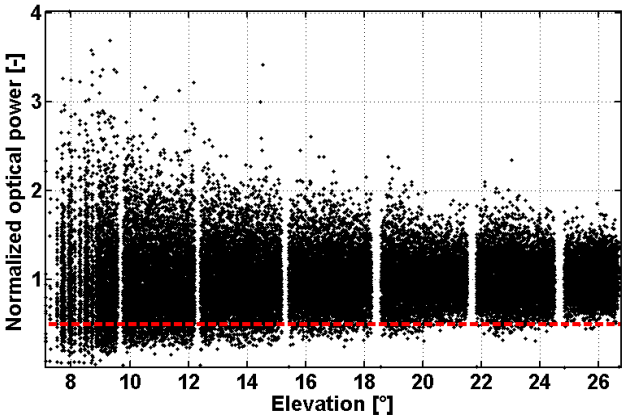

Fig. 3. Normalized received power over elevation at KT06-04. The black values are the normalized power samples recorded at 10 kHz rate. The dashed red line marks the -3 dB threshold with respect to unity mean [7].

The auto-correlation function (ACF) of the power vector in Fig. 3 is shown in Fig. 4 for elevations of 10°, 15°, 20°, and 25°. With increasing angle, the function becomes more and more narrow, indicating faster fluctuations. Especially the slew rates rising with elevation influence this behavior. Fig. 4 also illustrates the definition of auto-correlation time τ_c [s] (ACT) of received power defined as the 50 % roll-off of the ACF, i.e. the half width at half maximum of the function. The legend in Fig. 4 gives the related values for τ_c.

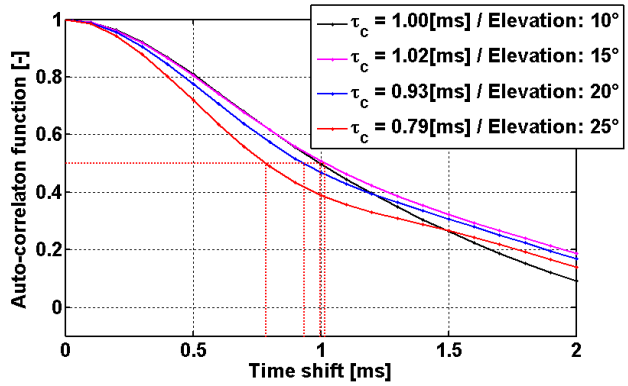

Fig. 4. Auto-correlation functions for selected elevations in KT06-04. The dashed red lines denote the 50% roll-offs [7].

The normalized power spectral density (PSD) as the Fourier transform of the ACF is plotted in Fig. 5 for 10°, 15°, 20°, and 25° elevation. No strong difference can be observed for the cut-off frequency as also expected from the rather small differences in correlation time. The auto-correlation time and the quasi-frequency over elevation are shown in Fig. 6. Since the first is proportional to the width of the ACF and the second to the width of the PSD, the runs of the curves are complementary.

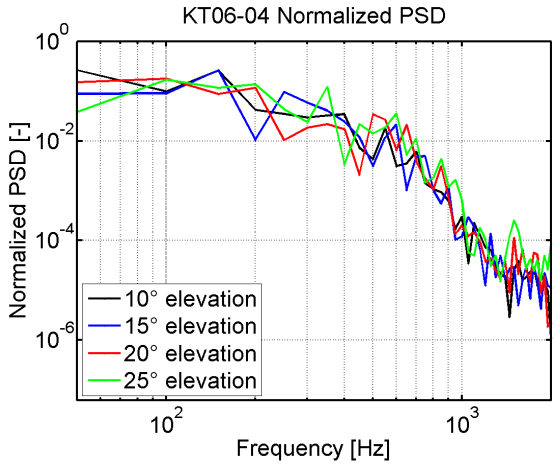

Fig. 5. Power spectral density for selected elevations in KT06-04.

The ACT is varying between 0.5 and 1.2 ms, the quasi-frequency between 400 and 600 Hz. For both parameters, a global maximum and a global minimum can be observed, respectively, at the same elevation. The cause is the varying atmospheric path length and accompanying saturation at a particular point and the slew rate of the satellite as seen from the ground station.

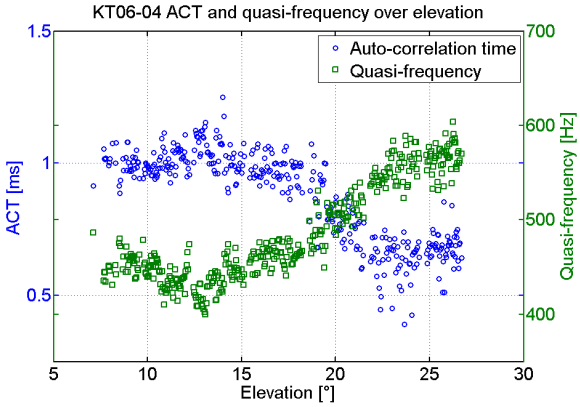

Fig. 6. Auto-correlation time and quasi-frequency over elevation for KT06-04.

The power scintillation index and the fractional fade time (with -3 dB threshold), as fluctuation frequency independent parameters, are plotted over elevation in Fig. 7. The span of σ_P^2 is from 0.3 to 0.03 along with Pr(P<=P_T) from 25 % to 0.02 %.

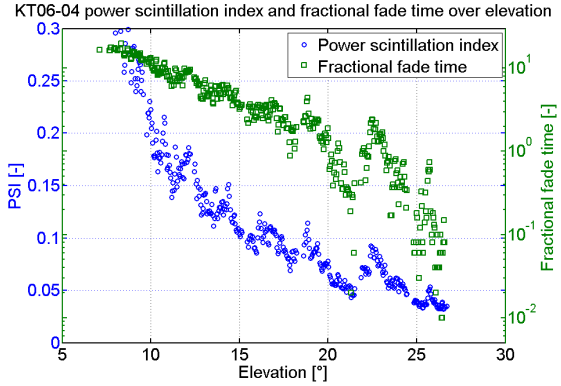

Fig. 7. Power scintillation index and probability of fade over elevation for KT06-04.

Please note here, that Pr(P<=P_T) is independent of the quasi-frequency and therefore only determined by the power scintillation index. Eventually, by knowing σ_P^2 (Fig. 7) and υ_0 (Fig. 6), $\langle n(P_T)\rangle$, Pr(P<=P_T) and $\langle t(P_T)\rangle$ can be determined with equation [1], [4], [5]. In contradiction to Pr(P<=P_T), $\langle n(P_T)\rangle$ has direct and $\langle t(P_T)\rangle$ indirect dependency on the quasi-frequency and also depends on σ_P^2. The course over elevation for KT06-04 is shown in Fig. 8.

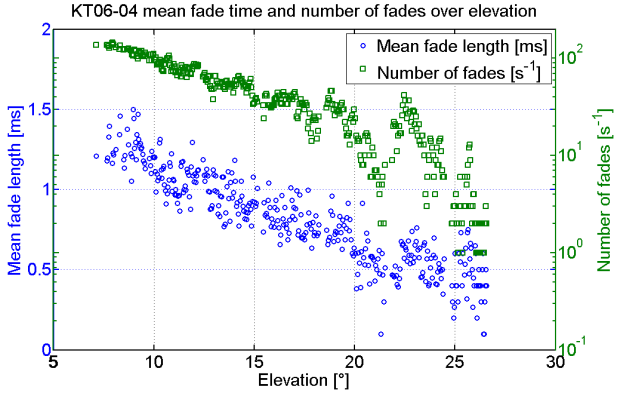

Fig. 8. Mean fade length and number of fades over elevation for KT06-04.

Aside the expectations of fade statistics, the distribution of fade length is of special interest. The cumulative density functions (CDF) of fade length for 10°, 15°, 20°, and 25° elevation are shown in Fig. 9. The step shape of the lines is owed to the measurement sampling time (10 kHz). In tendency, the fade are longer for low elevations. At 10° elevation, 90% of the fades are shorter than 2.4 ms. This 90%-probability drops down to 1.9 ms at 20°, 1.1 ms at 15°, and 0.9 ms at 10°.

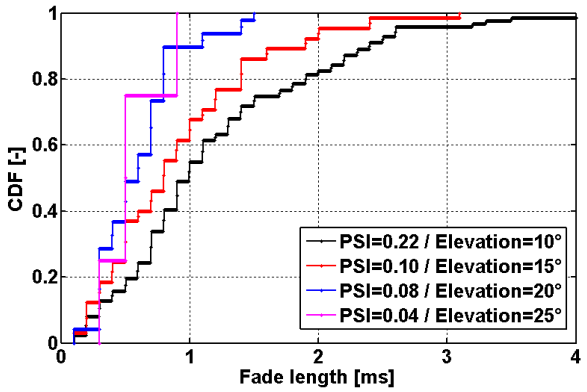

Fig. 9. Cumulative distribution functions for selected elevations in KT06-04. The fade threshold is defined as 3 dB below instantaneous mean.

B. *Overview of experiment results over elevation*

Similar to the illustration in the preceding chapter, the overview plots over elevation for all trials are shown here. The auto-correlation time is shown in Fig. 10. The values lie approximately in the interval between 0.5 and 2.0 ms. The global maximum similar to Fig. 6 can be also seen here for experiments KT06-03, KT06-04 and KT09-05. The run of the quasi-frequency over elevation for all measurements can be seen in Fig. 11. The values range from ~400 Hz up to 1200 Hz. The global minimum can be clearly seen for KT06-04. However, this is not very distinct for the other experiments.

Especially in KT06-02 the behavior is odd which cannot be explained to far. The power scintillation index is plotted in Fig. 13. The run is monotonously decreasing with elevation from ~0.4 to even below 0.05 for some trials.

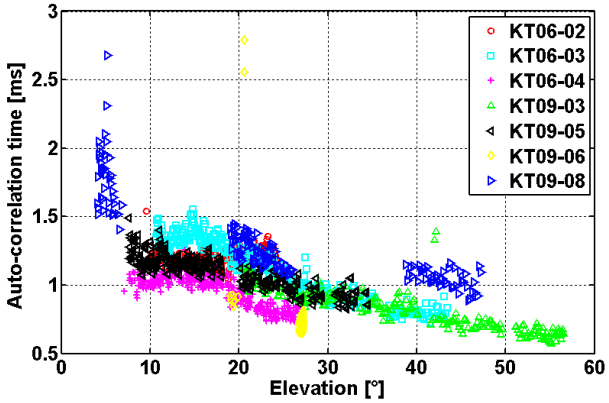

Fig. 10 Auto-correlation time over elevation for all KIODO measurements as defined by the 50% roll-off of the auto-correlation function.

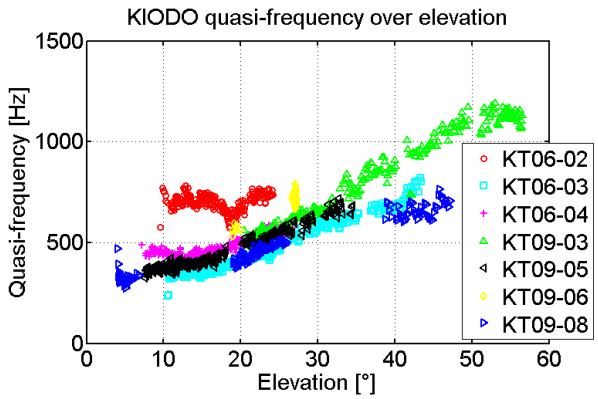

Fig. 11 Quasi-frequency over elevation for all KIODO measurements.

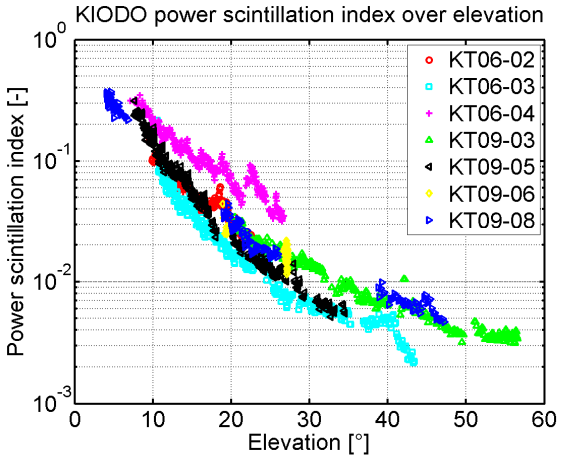

Fig. 12 Number of fades per second over elevation for all KIODO measurements. The fade threshold is defined as 3dB below instantaneous mean [7].

The quasi-frequency and the power scintillation index are related to the fade number per time, depicted in Fig. 13. The span is from 150 fades per second down to below one per second. The mean fade length is shown in Fig. 14. Values between 0.1 and 2.2 ms occur. The fractional fade time is depicted in Fig. 15. Note that this parameter does not depend on time behavior.

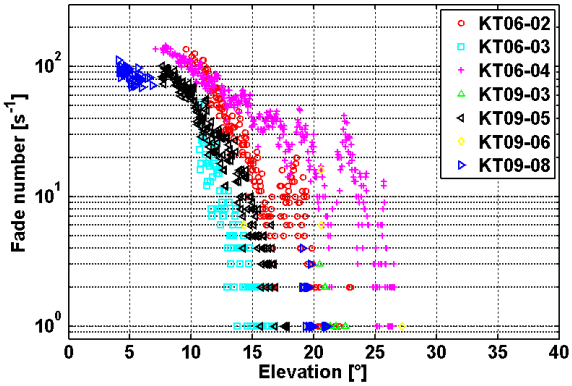

Fig. 13 Number of fades per second over elevation for all KIODO measurements. The fade threshold is defined as 3dB below instantaneous mean [7].

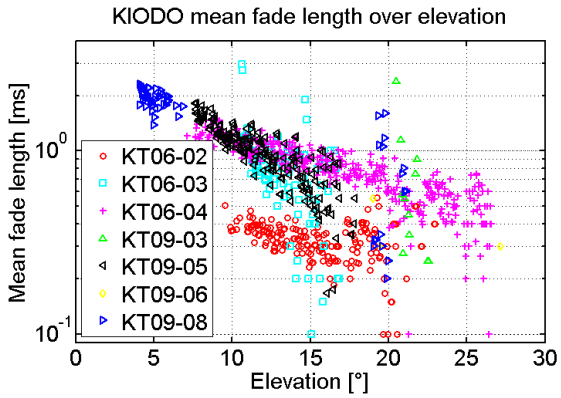

Fig. 14 Mean fade length over elevation for all KIODO measurements. The fade threshold is defined as 3dB below instantaneous mean.

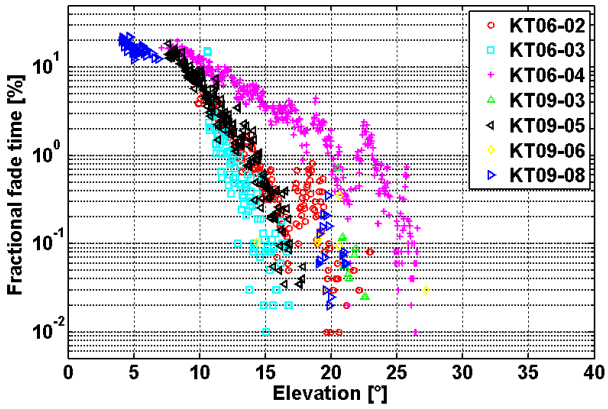

Fig. 15 Fractional fade time over elevation for all KIODO measurements. The fade threshold is defined as 3dB below instantaneous mean [7].

C. *Overview of experiment results over slew rate*

Similar to the illustration in the preceding chapter, the overview plots over slew rate for all trials are shown here. This illustration reveals the dependency of the particular time dependent statistics on slew rate and therefore, the time

behavior due to transversal pseudo-wind. Fig. 16, Fig. 17, Fig. 18, and Fig. 19 show the auto-correlation time, the quasi-frequency, the fade number and the mean fade duration over slew-rate. Neither τ_c, nor $\langle n(P_T)\rangle$ nor $\langle t(P_T)\rangle$ have clear exclusive dependency on the slew rate, i.e. show homogenous shape of the runs. Thus, the additional dependence on elevation still seems to be very high.

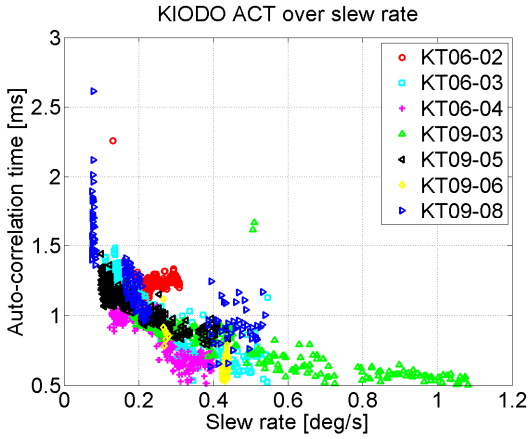

Fig. 16 Auto-correlation time over slew rate for all KIODO measurements as defined by the 50% roll-off of the auto-correlation function.

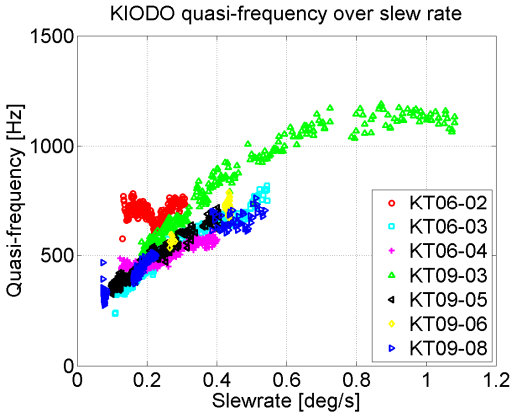

Fig. 17 Quasi-frequency over slew rate for all KIODO measurements.

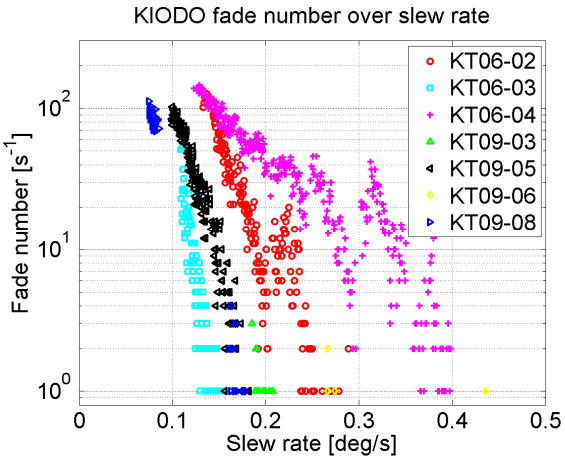

Fig. 18 Number of fades per second over slew rate for all KIODO measurements. The fade threshold is defined as 3dB below instantaneous mean.

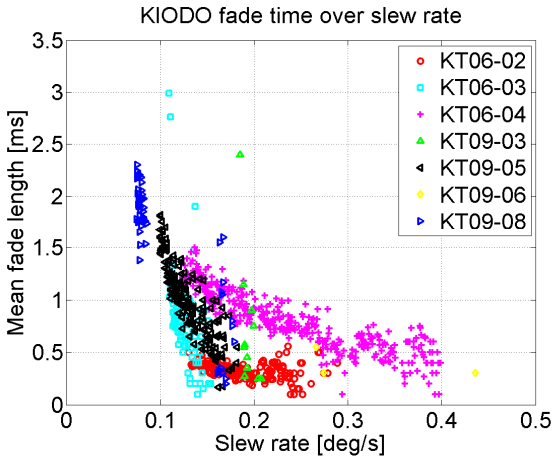

Fig. 19 Mean fade duration over slew rate for all KIODO measurements. The fade threshold is defined as 3dB below instantaneous mean.

V. MODELLING USE OF THE MEASUREMENTS

Neither the illustration over elevation nor the illustration over slew-rate seems to give satisfying homogeneity in the run of the individual measurement curves. However, this is needed for a useful measurement based modelling approach, e.g. when it is necessary to identify a representative mean out of a particular array of curves with reasonable confidence intervals. An approach on how to deal with this problem is given here for the auto-correlation time of received power. It makes sense to begin with this parameter since it is of high interest and practical value because it can be directly used to estimate size of interleavers and buffers in communication system design. Furthermore, it may be used to describe the ACF and thus the quasi-frequency, which in turn is exploited to calculate the fade statistics. As evident in Fig. 6 and Fig. 10, τ_c has a global maximum which drops down to its right towards higher elevations and to its left towards lower elevation. The drop on the right is assumed to be caused by the stronger influence of the slew rate. The drop to the left is due to the impact of the turbulence. The global maximum is expected to shift with different maximal elevation of the particular overflight, i.e. from overflight to overflight. Therefore, much information would be lost when averaging or fitting over the mean of the measurements for a suitable analytical description. An approach to overcome this problem is trying to separate the influence of slew rate and plain turbulence to result in a more suitable array of curves for the modelling. A straight forward approach is normalization (scaled) by the slew rate. When the auto-correlation time over elevation α [°] is divided by the slew rate SR [°/s] over elevation of the individual overflight, one obtains the normalized auto-correlation time $\tau_{c,n}$ [s/(°s^{-1})]

$$\tau_{c,n}(\alpha) = \frac{\tau_c(\alpha)}{SR(\alpha)}, \qquad [6]$$

which is shown in Fig. 20. The run of the curves here is more homogeneous than the in Fig. 10. Modelling with an exponential fit seems to be feasible. This model would describe a scaled auto-correlation time over elevation being independent of instantaneous slew-rate. For prediction of τ_c, $\tau_{c,n}$ would be determined with the modeled description and weighted with the

deterministic slew rate of a particular satellite overflight. Note that in this approach, the different cases of weak, moderate and strong fluctuations are not considered yet. Furthermore, the direct use of the slew rate as normalization function is a first order assumption. The treatment with the pseudo-transversal wind speed at the volumes of most impact of the turbulence (in some distance of the receiver) should give a more accurate description. Furthermore, the impact of different wind directions and amplitude was neither taken into account.

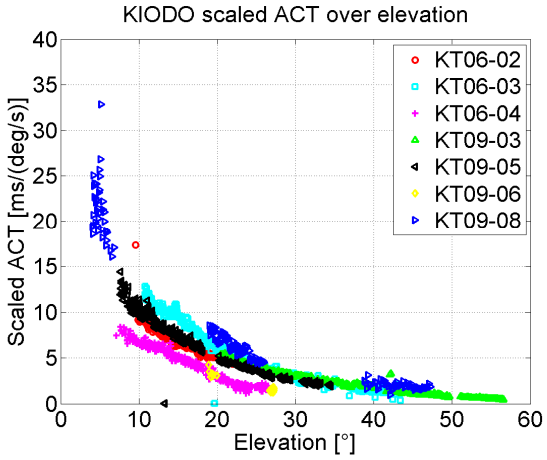

Fig. 20 Scaled auto-correlation time over elevation.

This modelling approached may also be applied to translate the modeled parameter, like the auto-correlation time, which is based on measurements from a specific location to any other location. In the same way as normalization is performed with the slew rate in the actual example, a suitable parameter describing the cumulated effect of turbulence over elevation can be used to normalize the measured parameter with the run of cumulated turbulence of the measurement location and de-normalize it with the run of particular location of interest. The Fried parameter seems to be feasible for that matter since it contains an integral over the un-weighted path profile of the index of refraction structure parameter. Alternatively, the plain integral can also be used for normalization. What is more, similar methods can be used to translate to other apertures and wavelengths.

VI. CONCLUSION

An analysis of the time and fading behavior of the turbulence in the LEO downlink scenario is presented. Detailed explanation is given for a single example satellite pass, as well as overview results displayed over link elevation and instantaneous slew rate of a range of passes. It can be seen that neither exclusive dependence on elevation nor on slew rate is occurs. Therefore, a first model approach to separate the combined effects of turbulence and slew rate with advantages and limitations are discussed. This model approach will be further investigated, refined and tested for practical use and physical compliance in subsequent publications.

ACKNOWLEDGMENT

The author wants to thank all staff members who made contributed to preparation, conduction and analysis of the KIODO measurement campaigns: Martin Brechtelsbauer, Christian Fuchs, Dr. Dirk Giggenbach, Joachim Horwath, Dr. Markus Knapek, and Dr. Nicolas Perlot.

REFERENCES

[1] F. G. Smith, Atmospheric propagation of radiation - the infrared and electro-optical systems handbook. Bellingham: SPIE Press, 1996.

[2] L. C. Andrews and R. L. Philips, Laser beam propagation through random media. Bellingham: SPIE Press, 2005.

[3] L. C. Andrews, R. L. Phillips, and C. Y. Hopen, "Scintillation model for a satellite communication link at large zenith angles," in SPIE Optical Engineering, Volume 39, pp. 3272 – 3280, 2000.

[4] M. Toyoshima, H. Takenaka, and Y. Takayama, "Atmospheric turbulence-induced fading channel model for space-to-ground laser communications links," in OSA Optics Express, Volume 19, Issue 17, pp. 15965-15975, 2011.

[5] N. Perlot, M. Knapek, D. Giggenbach, J. Horwath, M. Brechtelsbauer, Y. Takayama, and T. Jono," Results of the optical downlink experiment KIODO from OICETS satellite to optical ground station Oberpfaffenhofen (OGS-OP)", in Proceedings of SPIE, vol. 6457, 2007, pp. 645704-1 - 645704-8.

[6] N. Perlot, "The Kirari optical downlink to Oberpfaffenhofen (KIODO)," German Aerospace Center (DLR), Weßling, Germany, Report on DLR-JAXA Joint Experiment, 2007.

[7] F. Moll and M. Knapek, "Free-space laser communications for satellite downlinks: Measurements of the atmospheric channel," in Proceedings of the 62nd International Astronautical Congress, 2011.

[8] D. Giggenbach, F.Moll, and N. Perlot, "International campaign of laser communication experiments using OICETS - optical communication experiments at DLR," in NICT journal, 2012.

[9] Y. Takayama et al.,"Expanded laser communication demonstration with OICETS and ground stations", in Proceedings of SPIE, vol. 7587, 2010, pp. 75870D-1 - 75870D-8.

[10] M. Toyoshima et al., "Ground-to-satellite laser communication experiments," in IEEE Aerospace and Electronic Systems Magazine, Volume 23, Issue 8, pp. 10-18, 2008.

[11] H. T. Yura and D. A. Kozlowski, "Low Earth orbit satellite-to-ground optical scintillation: comparison of experimental observations and theoretical predictions," in Optics Letters, Volume 36, Issue 13, 2011, pp. 2507-2509.

[12] M. Toyoshima, T. Sasaki, H. Takenaka, and Y. Takayama, "Scintillation model of laser beam propagation in satellite-to-ground atmospheric links," in Proceedings of the 62nd International Astronautical Congress, 2011.

[13] F. S. Vetelino, C. Young, L. Andrews, and J. Recolons, "Aperture averaging effects on the probability density of irradiance fluctuations in moderate-to-strong turbulence," in Applied Optics, Volume 46, Issue 11, pp. 2099-2108, 2007.

[14] F. E. Strömqvist Vetelino, "Fade statistics for a lasercom system and the joint PDF of a gamma-gamma distributed irradiance and its time derivative," Ph.D. dissertation, University of Central Florida, Orlando, Florida, USA, 2006.